Conductance of Photons in Disordered Photonic Crystals

A. A. Asatryan, L. C. Botten, T. N. Langtry,
Department of Mathematical Sciences, University of Technology, Sydney, N.S.W. 2007, Australia

R.C. McPhedran, C. Martijn de Sterke, P. A. Robinson
School of Physics, University of Sydney, NSW 2006, Australia

The conductance of photons in two-dimensional disordered photonic crystals has been calculated using an exact multipole/plane wave method that includes all multiple scattering processes. The importance of evanescent coupling between adjacent layers is demonstrated and reveals that the widely used Pichard theory of electron conductance and the probability density distribution for the conductance of electrons based on the Dorokhov-Mello-Pereyra-Kumar equation do not apply to photons in a strongly scattering medium. The variance of the conductance is shown numerically to be independent of sample size for weak disorder, in accordance with the phenomenon of Universal Conductance Fluctuations established earlier for electrons. The conductance variance is also a strong function of disorder with the region of the Universal Conductance Fluctuation being very narrow. We show also that the relevant transfer matrix belongs to the class of complex symplectic matrices $Sp(2N, C)$.

PACS numbers: 42.25.Dd,42.25.Fx

The discovery of universal conductance fluctuations (UCF) of electrons [1], according to which the variance of the conductance g does not depend on the size or the degree of disorder of mesoscopic conductors, has led to considerable research [2] to understand the nature of such anomalously large fluctuations. A fundamental proposition [3] is that the statistical properties of conductance are governed by one of three standard random matrix ensembles classified by Dyson [4]: time reversal symmetry (orthogonal class), the absence of time reversal symmetry (unitary class), and broken spin symmetry (symplectic class) [2].

Since the scaling theory of Anderson localization [5] is based on the scaling properties of the averaged conductance $\langle g \rangle$, the discovery of UCF initiated a discussion about the validity of scaling theory itself, and it has been suggested that it should be reformulated in terms of conductance distributions $p(g)$ [6]. However, no such theory exists at this time. In quasi-1D systems, the evolution of $p(g)$ as a function of conductor length L is governed by the Dorokhov-Mello-Pereyra-Kumar (DMPK) equation [7]. This elegant theory was recently extended to higher dimensions [8] for broken time reversal symmetry. The electronic conductance distribution was calculated numerically [9] for both insulating and metallic regimes and at the mobility edge [10, 11]. Subsequently, non-analytic behavior of $p(g)$ was reported at the crossover point on the mobility edge ($g \approx 1$) [12]. Despite substantial research, complete characterization of the conductance distribution remains open.

Originally developed to describe the transport properties of electrons in disordered wires, the concept of conductance can also be applied to photons [13]. Calculations of $p(g)$ have been reported in the diffusive approximation [14], using random matrix theory [15] and for surface corrugated waveguides [16]. The distribution of the photon conductance was also investigated experimentally [17]. In the diffusive regime $p(g)$ is approximately Gaussian, while in the strong scattering regime ($g \ll 1$), theory [14, 15] and experiment [18] are consistent. To date, however, none of the models for the conductance distribution for dimensions $d \geq 2$ with bulk defects have fully incorporated multiple scattering. Here we undertake such a calculation. While the modelling of non-interacting photons differs from that electrons, the majority of electronic models do not take into account electron-electron interactions. Accordingly, the results obtained in the photon case could be also relevant to electrons.

Our aim here is to investigate the conductance fluctuations of photons and its distribution for two-dimensional disordered photonic crystals. Our calculations are based on the exact method of multipole expansions and include rigorously all scattering orders. It comprises both the microscopic approach [1], where the multiply scattered field is calculated exactly for single layers (taking into account all scattering events), and macroscopic approach [7] in which these layers are stacked using exact recurrence relations. We calculate the conductance of a bulk, disordered, photonic crystal and investigate the effects of the degree of disorder and sample size on the conductance, its fluctuations, and its distribution at the crossover region ($g \approx 1$). This reveals the importance of evanescent wave contributions, which in turn makes the Pichard formulation of conductance and the DMPK equation not directly applicable to photons in the strong scattering regime, given that these only incorporate propagating plane wave terms.

We consider a two-dimensional, disordered photonic crystal, each layer of which is a cylinder diffraction grat-

ing with a supercell periodically replicated. The supercell comprises a set of N_c infinitely long cylinders of radii a_l, refractive indices n_l, with centers located at $\mathbf{c}_l$. The properties of each grating layer are then computed rigorously using a multipole method from which plane wave scattering matrices that characterize the action and interaction of each grating layer are calculated [19]. The scattering matrices of the individual grating layers are then coupled using recurrence relations to yield the transmission ($\mathbf{T}$) and reflection ($\mathbf{R}$) scattering matrices for a slab of N_L layers [19]. The elements of these matrices, for example T_{pq}, express the amplitudes transmitted (and reflected) into channel p given unit amplitude incidence in channel q. Since the problem is formulated in terms of diffraction gratings with a common supercell period, the channels are represented by the set of diffracted orders which comprise a finite number of propagating orders and an infinite number of evanescent orders.

While any of the $\mathbf{c}_l$, a_l and n_l can be randomized, the results here are for random n_l, uniformly distributed in $[\bar{n}-Q, \bar{n}+Q]$. We take $N_c = 21$, which is sufficient for supercell effects to be negligible. The structure is irradiated with a normal incident plane wave, with the electric field aligned with the cylinder axes (E polarized).

The dimensionless conductance of the sample is given by the generalized two-terminal Landauer formula [20] for multichannel propagation

$$g = \sum_p \sum_q |T_{pq}|^2 = \mathrm{Tr}\ \mathbf{T}\mathbf{T}^\dagger = \mathrm{Tr}\ \mathbf{T}^\dagger\mathbf{T}. \qquad (1)$$

Here, $|T_{pq}|^2$ denotes the transmitted flux in channel p associated with unit flux in channel q, with the summation in (1) being taken over all propagating plane waves.

The matrices $\mathbf{R}$ and $\mathbf{T}$ are infinite and must be truncated in any numerical implementation, with the truncation order determined by convergence studies. We retain plane wave orders $[-N_t, N_t]$, ensuring that this set includes all propagating channels and as many evanescent channels as required for convergence. The conductance is computed by summing the square magnitudes $|T_{pq}|^2$ associated with all propagating input and output channels (1).

To demonstrate the importance of the evanescent wave coupling we show in Fig. 1 the conductance versus the stack length N_L for a single realization with the inclusion of evanescent fields sufficient for convergence (solid line), and without evanescent coupling, using only propagating channels (dashed line). Throughout we model a square lattice with lattice constant d, and cylinders of fixed normalized radius $a_l/d = 0.3$, and $\bar{n} = 3$. The wavelength is $\lambda = 2.21d$, located in the pass band between the first two gaps of the associated regular photonic crystal. Fig. 1 shows that the evanescent field is important for characterizing the conductance. Note that in the localized regime ($g \lesssim 1$), transport is mainly determined by the evanescent coupling.

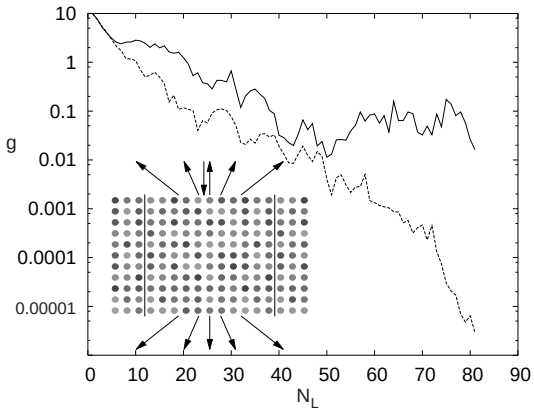

FIG. 1: Conductance g versus the number of layers N_L for a single realization and $Q = 0.4$. Solid line: evanescent coupling included ($N_t = 50$); dashed line: only propagating orders included ($N_t = 9$). The inset depicts the diffraction geometry and displays a supercell of a random stack upon which is incident a single plane wave field from above which gives rise to reflected and diffracted plane wave orders.

The conductance g and its distribution $p(g)$ can be calculated from the transfer matrix $\mathcal{T}$ [2] which connects the field on either side of the stack. It has the form

$$\boldsymbol{\mathcal{T}} = \begin{bmatrix} \mathbf{T} - \mathbf{R}'\mathbf{T}'^{-1}\mathbf{R} & \mathbf{R}'\mathbf{T}'^{-1} \\ -\mathbf{T}'^{-1}\mathbf{R} & \mathbf{T}'^{-1} \end{bmatrix}, \qquad (2)$$

where $\mathbf{R}$, $\mathbf{T}$ and $\mathbf{R}'$, $\mathbf{T}'$ are the amplitude reflection and transmission matrices, respectively for incidence from above and below (see the inset of Fig. 1), and include both propagating and evanescent components. The evanescent terms substantially alter the properties of $\boldsymbol{\mathcal{T}}$ upon which the Pichard treatment of conductance relies.

¿From reciprocity [22], it follows that $\boldsymbol{\mathcal{T}}'^T = \boldsymbol{\sigma}_x\mathbf{T}\boldsymbol{\sigma}_x$, $\mathbf{R}^T = \boldsymbol{\sigma}_x\mathbf{R}\boldsymbol{\sigma}_x$ and $\mathbf{R}'^T = \boldsymbol{\sigma}_x\mathbf{R}'\boldsymbol{\sigma}_x$. Here, the superscripted T indicates matrix transposition and $\boldsymbol{\sigma}_x = \boldsymbol{\sigma}_x{}^{-1}$ denotes the first Pauli matrix of dimension $2N_t+1$, comprising unit elements on the secondary diagonal. These relations, which hold analytically within the multipole based formulation, are then sufficient to establish that

$$\boldsymbol{\mathcal{T}}^T\boldsymbol{S}\boldsymbol{\mathcal{T}} = \boldsymbol{\mathcal{T}}\boldsymbol{S}\boldsymbol{\mathcal{T}}^T = \mathbf{S}, \qquad (3)$$

also holds analytically within the formulation. In (3)

$$\mathbf{S} = \begin{bmatrix} \mathbf{0} & \boldsymbol{\sigma}_x \\ -\boldsymbol{\sigma}_x & \mathbf{0} \end{bmatrix}. \qquad (4)$$

Thus, the transfer matrix for photons belongs to the class of complex symplectic matrices $Sp(2N, C)$ [4].

¿From generalized energy conservation relations [19] it follows that the transfer matrix satisfies the relation [22]

$$\boldsymbol{\mathcal{T}}^\dagger \begin{bmatrix} \mathbf{I}_p & -i\mathbf{I}_e \\ i\mathbf{I}_e & -\mathbf{I}_p \end{bmatrix} \boldsymbol{\mathcal{T}} = \begin{bmatrix} \mathbf{I}_p & -i\mathbf{I}_e \\ i\mathbf{I}_e & -\mathbf{I}_p \end{bmatrix}, \qquad (5)$$

where $\mathbf{I}_p$ and $\mathbf{I}_e$ are matrices of size $2N_t + 1$, with all elements set to zero except for those on the primary diagonal which are set to unity respectively for propagating and evanescent channels. This is the generalized energy conservation relation satisfied by the transfer matrix for photons. Note that the scattering matrix connecting the amplitudes in the incoming channels to the outgoing channels, and which includes both propagating and evanescent orders, is not unitary[19], in contrast to the electronic case. Combining (3) and (5), we derive

$$\boldsymbol{\mathcal{T}}^* = \begin{bmatrix} i\mathbf{I}_e\boldsymbol{\sigma}_x & \mathbf{I}_p\boldsymbol{\sigma}_x \\ \mathbf{I}_p\boldsymbol{\sigma}_x & i\mathbf{I}_e\boldsymbol{\sigma}_x \end{bmatrix} \boldsymbol{\mathcal{T}} \begin{bmatrix} i\mathbf{I}_e\boldsymbol{\sigma}_x & \mathbf{I}_p\boldsymbol{\sigma}_x \\ \mathbf{I}_p\boldsymbol{\sigma}_x & i\mathbf{I}_e\boldsymbol{\sigma}_x \end{bmatrix}^{-1}, \qquad (6)$$

a consequence of time reversal invariance. Here, the superscripted asterisk denotes complex conjugation. The distribution of $p(g)$ and the conductance g itself depend on these general properties of $\boldsymbol{\mathcal{T}}$.

The starting point in determining g and its distribution $p(g)$ in Pichard's treatment [2] is the polar decomposition of the transfer matrix $\boldsymbol{\mathcal{T}}$

$$\boldsymbol{\mathcal{T}} = \begin{bmatrix} \mathbf{u}_1\sqrt{\mathbf{1}+\boldsymbol{\lambda}}\mathbf{u}_2 & \mathbf{u}_1\sqrt{\boldsymbol{\lambda}}\mathbf{u}_2^* \\ \mathbf{u}_1^*\sqrt{\boldsymbol{\lambda}}\mathbf{u}_2 & \mathbf{u}_1^*\sqrt{\mathbf{1}+\lambda}\mathbf{u}_2^* \end{bmatrix}, \qquad (7)$$

where the $\mathbf{u}_i$ are unitary matrices, and $\boldsymbol{\lambda}$ is a real diagonal matrix. This parametrization derives from the singular value decomposition of the respective block matrices in (2). While this structure is valid for matrices that include only propagating states, the substantial differences in the structure of the time reversal invariance equations (5) and (6) due to the evanescent terms represented by $\boldsymbol{I}_e$, mean that the decomposition (7) is not valid. In particular, the singular values are not the same for the block matrices $\mathcal{T}_{11}$, $\mathcal{T}_{22}$ and $\mathcal{T}_{12}$, $\mathcal{T}_{21}$. Hence, the Pichard and DMPK formulations are not valid in their present form when evanescent waves, needed for accurate characterization of the photon conductance, are incorporated.

We now turn to the average conductance and its fluctuations. In Fig. 2 we show the average conductance $\langle g\rangle$ versus the number of layers N_L for three values of Q. The maximum stack length is $N_L = 81$, so that, with $N_c = 21$, there are 1701 cylinders per sample. Averages were taken over 4900 realizations which is sufficient for the calculation ensemble means stable to 3 significant figures. Three wave propagation regimes, which are more prominent for strong disorder (dotted line Fig. 2), are found. The propagation and transition regimes occur respectively for $N_L \lesssim 10$ and $10 \lesssim N_L \lesssim 20$ layers, while for longer stacks ($N_L \gtrsim 20$) the linear behaviour points to the onset of Anderson localization (Fig. 2). For strong disorder ($Q = 1.5$), this transition requires fewer layers than for weak disorder.

According to the Thouless estimate [21], localization sets in when $g \leq 1$, while for $g > 1$, waves are delocalized. In Fig. 2, we observe transitions to the linear regime

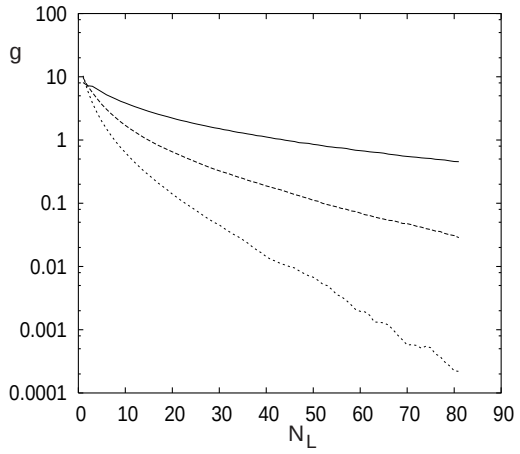

FIG. 2: Conductance $\langle g\rangle$ versus size of the cluster N_L for different degrees of disorder: $Q = 0.2$ (solid line), $Q = 0.4$ (dashed line), $Q = 1.5$ (dotted line)

.

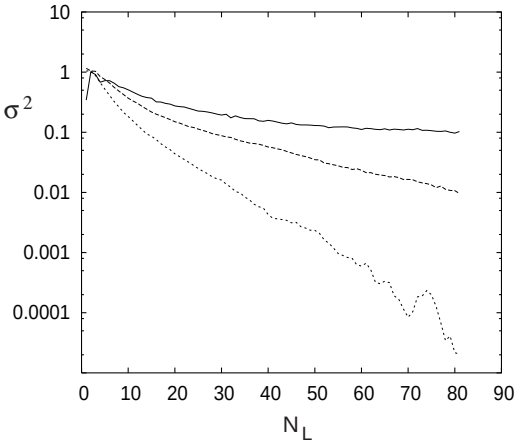

FIG. 3: Variance σ^2 versus cluster size N_L for different degrees of disorder: $Q = 0.2$, 0.4, and 1.5 from top to bottom.

commencing at $g \approx 2,\ 0.6$ and 0.2, for $Q = 0.2, 0.4, 1.5$ respectively, consistent with the Thouless criterion [21].

It is also known [1] that for weak disorder the sample exhibits universal conductance fluctuations according to

$$\sigma^2 = \langle g^2\rangle - \langle g\rangle^2 \approx \text{const}, \qquad (8)$$

a result that depends neither on the degree of disorder nor on the sample size. Fig. 3 shows the variation of the variance σ^2 of the conductance with the number of layers. For weak disorder, σ^2 does not depend on the number of layers (top curve), while for stronger disorder it appears that the variance decreases in the localization regime. This is similar to the electronic case. In Fig. 4 we show the variance σ^2 versus the degree of disorder Q, and note that σ^2 depends strongly on the disorder with universal conductance fluctuations being observed only in the range $0.15 < Q < 0.2$.

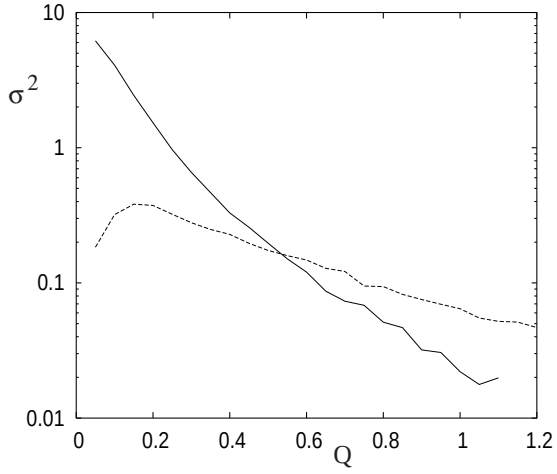

FIG. 4: Variance σ^2 versus Q for different samples sizes: $N_L = 25$ (solid line), $N_L = 15$ (dashed line).

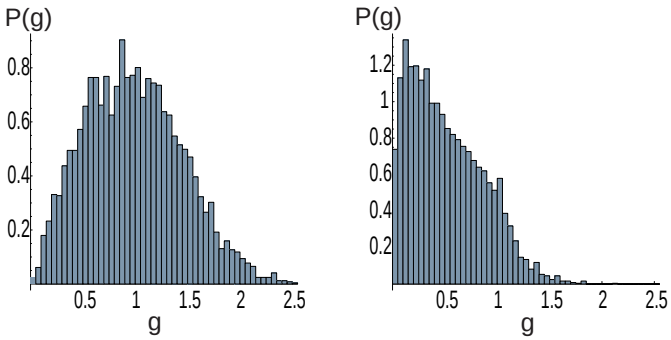

FIG. 5: Conductance distribution $p(g)$ at $\langle g\rangle = 0.98$ and $\langle g\rangle = 0.51$.

Finally, in Fig. 5 we show the distribution $p(g)$ for the averaged conductances $\langle g\rangle = 0.98$ and $\langle g\rangle = 0.51$ respectively. Despite reports [12] of non-analytic behavior of $p(g)$ in the crossover region ($g \approx 1$), we do not observe such behavior; the incorporation of the evanescent terms may have smoothed this transition.

In conclusion, we have calculated using an exact numerical method the conductance of a disordered, two-dimensional photonic crystal comprised of circular cylinders. The results emphasize the importance of evanescent coupling for photon conductance and indicate in the localization regime the conductance is governed by this evanescent coupling. The inclusion of this coupling necessitates a reformulation of the Pichard formalism and the DMPK equation which incorporate only to propagating states. Universal conductance fluctuations for photons are also explicitly demonstrated. We show that the variance of the conductance does not depend on the sample size for weak disorder, similar to the electronic case, while for fixed sample size it is a strong function of disorder, in contrast to the electronic case. It is suggested that the inclusion of evanescent coupling smooths the conductance distribution in the transition region.

The work was produced with the assistance of the Australian Research Council. We also acknowledge computing support from the Australian Centre for Advanced Computing and Communication (ac3) and the Australian Partnership for Advanced Computing (APAC).

[1] P.A.Lee, A.D.Stone, Phys. Rev. Lett. **55**, 1622-1625 (1985); B.L.Altschuler, JETP Lett. **41**, 648-651 (1985).
[2] *Mesoscopic Phenomena in Solids*, Eds. B.L. Altshuler, P.A.Lee, R.A. Webb (North-Holland, Amsterdam, 1991).
[3] Y.Imry, Europhys. Lett. **5**, 249 (1986).
[4] F.J.Dyson, J. Math. Phys,**3**, 140 (1962); ibid **3**, 157 (1962); ibid **3**, 166 (1962).
[5] E.Abrahams, P.W.Anderson, D.C.Licciardello, and T.V. Ramakrishnan, Phys. Rev. Lett. **42**, 673-676 (1979).
[6] B.Shapiro, Phys.Rev. B **34**, 4394 (1986).
[7] P.A.Mello, P.Pereyra, and N.Kumar, Ann. Phys.(N.Y.) **181**, 290 (1988); O.N.Dorokhov, JETP Lett. **36**, 318 (1982); K.A.Muttalib, J.-L. Pichard, A.D. Stone, Phys. Rev. Let. **23**, 2475 (1987).
[8] K.A.Muttalib, and V.A.Gopar, Phys. Rev. B **66**, 115318 (2002).
[9] V.Plerou, and Z.Wang, Phys. Rev. B **15**, 1967 (1998).
[10] P.Markos, Phys. Rev. Lett. **83**, 588 (1999); C.M. Soukoulis, X. Wang, Q. Li, and M.M. Sigalas, Phys. Rev. Lett. **87**, 668 (1999).
[11] M. Rühländer, P. Markos, and C.M. Soukoulis, Phys. Rev. B **64**, 212202 (2002).
[12] K.A. Muttalib, P. Wölfle, Phys. Rev. Lett. **83** 3013 (1999); K.A. Muttalib, P. Wölfle, A. Garcia-Martin, and V.A. Gopar, Europhys. Lett. **61**, 95 (2003).
[13] S. Feng, C. Kane, P.A. Lee, A.D. Stone, Phys. Rev. Lett. **61**, 834 (1988); P. Sheng *Scattering and Localization of classical waves in Random Media* (World Scientific, Singapore, 1990)
[14] Th. M. Nieuwenhuizen, and M.C.W. van Rossum, Phys. Rev. Lett. **74**, 2674 (1995).
[15] E. Kogan, and M. Kaveh, Phys. Rev. B, **52** 3813 (1995)
[16] A. Garcia-Martin, and J.J. Saenz, Phys. Rev. Lett. **87**, 116603 (2001).
[17] J.F. de Boer, M.C. W. van Rossum, M.P. van Albada, Th.M. Nieuwenhuizen, and Ad. Lagendijk, Phys. Rev. Lett. **73**, 2567 (1994).
[18] M. Stoytchev, and A.Z. Genack, Phys. Rev. Lett. **79**, 309 (1997).
[19] L.C. Botten, N.A. Nicorovici, A.A.Asatryan, R.C. McPhedran, C.M. de Sterke, P.A. Robinson, J. Opt. Soc. Am A **17**, 2165 (2000); ibid **17**, 2177 (2000).
[20] D.S. Fisher, P.A. Lee, "Relation between conductivity and transmission matrix," Phys. Rev. B **23**, 6851-6854 (1981).
[21] D.J. Thouless, in Condensed Matter Ed. R. Balian, R. Maynard, and G. Toulouse (North Holland, Amsterdam, 1979), p. 43.
[22] L.C. Botten *et al.*, in preparation.